Developmental Biology 445 (2019) 80–89

Contents lists available at ScienceDirect

Developmental Biology

journal homepage: www.elsevier.com/locate/developmentalbiology

Novel components of germline sex determination acting downstream of *foxl3* in medaka

Mariko Kikuchi[a], Toshiya Nishimura[a], Daisuke Saito[b], Shuji Shigenobu[c,d], Ritsuko Takada[e,f], José Arturo Gutierrez-Triana[g,1], Juan Luis Mateo Cerdán[g,2], Shinji Takada[d,e,f], Joachim Wittbrodt[g], Mikita Suyama[b], Minoru Tanaka[a,*]

[a] Division of Biological Science, Graduate School of Science, Nagoya University, Nagoya 464-8602, Japan
[b] Division of Bioinformatics, Medical Institute of Bioregulation, Kyushu University, Fukuoka 812-8582, Japan
[c] Functional Genomics Facility, National Institute for Basic Biology, Okazaki 444-8585, Japan
[d] Department for Basic Biology, The Graduate University for Advanced Studies (SOKENDAI), Okazaki 444-8585, Japan
[e] Exploratory Research Center on Life and Living Systems, National Institutes of Natural Sciences, Okazaki 444-8787, Japan
[f] National Institute for Basic Biology, Okazaki 444-8787, Japan
[g] Department of Developmental Biology, Centre for Organismal Studies, University of Heidelberg, Im Neuenheimer Feld 230, 69120 Heidelberg, Germany

ARTICLE INFO

Keywords:
Germ cell
Sex determination
foxl3
Medaka
FOXL3-binding motif

ABSTRACT

Germline sex determination is an essential process for the production of sexually dimorphic gametes. In medaka, *Forkhead box L3* (*foxl3*) was previously identified as a germ cell-intrinsic regulator of sex determination that suppresses the initiation of spermatogenesis in female germ cells. To reveal the molecular mechanism of germline sex determination by *foxl3*, we conducted the following four analyses: Comparison of transcriptomes between wild-type and *foxl3*-mutant germ cells; epistatic analysis; identification of the FOXL3-binding motif; and ChIP-qPCR assay using a FOXL3-monoclonal antibody. We identified two candidate genes acting downstream of *foxl3*: *Rec8a* and *fbxo47*. It has been known that Rec8 regulates sister chromatid cohesion and Fbxo47 acts as a ubiquitin E3 ligase. These functions have not been, however, associated with sexual differentiation in germ cells. Our results uncover novel components acting downstream of *foxl3*, providing insights into the mechanism of germline sex determination.

1. Introduction

In vertebrates, including mammals and fish, it is generally accepted that sex determination of germ cells is influenced by somatic cell sex (Bowles and Koopman, 2010; Tanaka, 2016). However, the intrinsic mechanism of sex determination in germ cells largely remains unclear.

In mammals, early meiotic entry is a good indication of germ cell feminization. Retinoic acid (RA)-inducible gene, *Stra8* (*stimulated by retinoic acid 8*), controls the timing of meiotic entry in germ cells (Bowles and Koopman, 2007). A recent study in mice suggests that *Smad4* (*SMAD family member 4*), in conjunction with *Stra8*, regulates meiosis, and this activity correlates with the expression of oocyte marker genes (Miyauchi et al., 2017; Wu et al., 2016). In males, *Nanos2* (*nanos C2HC-type zinc finger 2*) has been shown to prevent germ cells from entering meiosis by controlling RA-susceptibility (Kato et al., 2015).

In the teleost fish medaka (*Oryzias latipes*) and zebrafish (*Danio rerio*), *nanos2* expression is detected in germline stem cells in both ovaries and testes (Aoki et al., 2009; Nakamura et al., 2010; Beer and Draper, 2013). Moreover, responsiveness to RA is detected not only in female but also in male germ cells during the critical period of germline sex determination in medaka (Adolfi et al., 2016). These data suggest that the initial event of germline sex determination is different among vertebrates, and that the commitment to meiosis and the establishment of germline stem cells should be considered distinct from germline sex determination (Tanaka, 2016).

Previously, *foxl3* (*Forkhead box L3*) was identified as an intrinsic factor for germline sex determination in medaka (Nishimura et al., 2015). *Foxl3*-expression is initially detected in both male and female germ cells, but is maintained only in female mitotic germ cells at later stages of gonadal sex differentiation. In the absence of *foxl3* function, XX germ cells produced functional sperm in the ovaries, indicating that

* Corresponding author.
E-mail address: mtanaka@bio.nagoya-u.ac.jp (M. Tanaka).
[1] **Present address** Escuela de Microbiología, Facultad de Salud, Universidad Industrial de Santander, Carrera 32 #29–31, Bucaramanga, Colombia.
[2] **Present address** Department of Information Technology, University of Oviedo, Calle Jesús Arias de Velasco, s/n, 33005 Oviedo, Asturias, Spain.

https://doi.org/10.1016/j.ydbio.2018.10.019
Received 22 August 2018; Received in revised form 8 October 2018; Accepted 23 October 2018
Available online 27 October 2018
0012-1606/

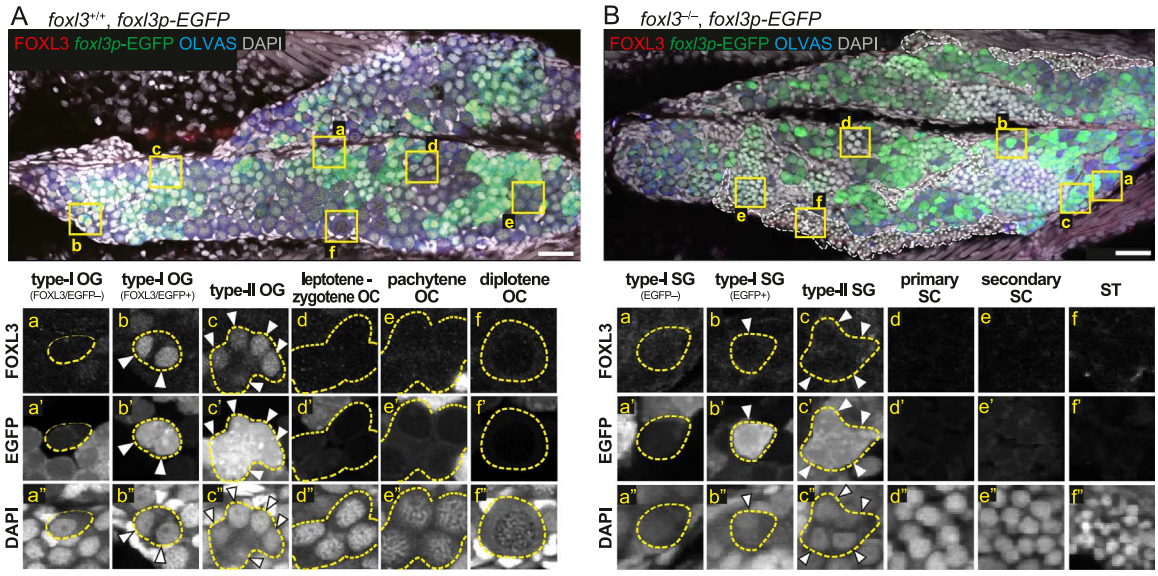

Fig. 1. Transcriptome analysis of *foxl3p-EGFP*-expressing cells isolated from wild-type and *foxl3*$^{-/-}$ ovaries. (A, B) Immunofluorescent staining for FOXL3 (red), EGFP (green), germ cell marker OLVAS (blue), and DAPI (gray) in 15 dph ovaries of wild-type (A) and *foxl3*$^{-/-}$ (B). White dashed lines in B indicate spermatids in the mutant ovaries. Different developmental stages of germ cells indicated by yellow boxes are magnified below (a-f). Yellow dashed line in the magnified images indicates a germ cell or a germline cyst (type II division). White arrowheads indicate EGFP positive germ cells. OG: oogonia, OC: oocyte, SG: spermatogonia, SC: spermatocyte, ST: spermatid. Bar: 30 μm. (For interpretation of the references to color in this figure legend, the reader is referred to the web version of this article).

foxl3 is required for suppression of spermatogenesis in female germ cells and that the sexual fate decision in germ cells occurs independently of somatic cell sex (Nishimura et al., 2015).

In this study, we focused on the pathways downstream of *foxl3*. *Foxl3* encodes a Forkhead transcription factor and is evolutionary conserved in vertebrates except for mammals (Bertho et al., 2016). Identification of the *foxl3*-downstream pathways will enable detailed analyses of the molecular mechanisms of germline sex determination and also provide insight into how conserved the intrinsic pathways of germline sex determination are among vertebrates.

2. Results

2.1. Transcriptome analysis of wild-type and *foxl3*$^{-/-}$ germ cells

To understand the molecular mechanisms of germline sex determination by *foxl3*, we examined the transcriptomes of wild-type and *foxl3*$^{-/-}$ (N-terminus 17 bp-deletion allele; Nishimura et al., 2015) germ cells. *Foxl3*-expressing germ cells were labeled using enhanced green fluorescent protein (EGFP) under the control of *foxl3*-promoter and *foxl3*-3′UTR (*foxl3p*-EGFP transgenics). EGFP expression was verified by immunohistochemistry of the ovaries at 15 day-post-hatching (dph) wild-type and *foxl3*$^{-/-}$ transgenics. At this stage, germ cells can be categorized into two types according to their modes of mitotic cell division (Saito et al., 2007). Type I germ cells, including germline stem cells, undergo self-renewal and are present in isolation, surrounded by supporting cells. Type II germ cells are gametogenesis-committed, and undergo several rounds of cyst-producing divisions, followed by meiosis. Endogenous *foxl3*/FOXL3-expression was detected in a subset of type I germ cells and all type II germ cells but was not detected in mitotically quiescent type I germ cells (Nishimura et al., 2015; Fig. 1A). The *foxl3p*-EGFP signal was also detected in a subset of FOXL3-positive type I germ cells and type II germ cells but not in another group of FOXL3-negative type I germ cells and meiotic oocytes (Fig. 1A). This indicates that the *foxl3p*-EGFP transgenics successfully reproduced the endogenous expression pattern of *foxl3*. As expected, EGFP signals were detected in a part of *foxl3*$^{-/-}$ mitotic germ cells (Fig. 1B).

Next, EGFP-positive germ cells were isolated from wild-type and *foxl3*$^{-/-}$ ovaries using a cell sorter (Sup. Fig. 1). The isolated germ cells were subsequently used for library preparation by a Quartz-seq method, a sensitive and quantitative method for RNA-sequencing with a small number of cells (Sasagawa et al., 2013). Correlation of the read coverage between wild-type (n = 3) and *foxl3*$^{-/-}$ (n = 3) was high (Sup. Fig. 2A; $r^2 > 0.94$), suggesting that the global gene expression of mitotic germ cells is similar between wild-type and *foxl3*$^{-/-}$ and that *foxl3* may modulate limited pathways to regulate the sexual fate of germ cells. Comparison of the transcriptomes between wild-type and *foxl3*$^{-/-}$ revealed 1480 differentially expressed genes (DEGs: false discovery rate (FDR) < 0.05). Among them, 600 and 880 genes were significantly upregulated in wild-type (DEG+) and *foxl3*$^{-/-}$ (DEG−) germ cells, respectively (Sup. Fig. 2B, Sup. Table 1). We did not find any RA-signaling-related DEGs in the list of functional annotation clustering of gene ontology terms (Sup. Table 2).

2.2. Screening of DEGs using *meioC*$^{-/-}$ ovaries

To obtain candidate genes acting downstream of *foxl3*, we examined the expression levels of DEG+ genes in wild-type and *meioC*$^{-/-}$ ovaries. In *meioC*$^{-/-}$ ovaries, a subset of type I germ cells expressed FOXL3, but did not develop beyond type I (Nishimura et al., 2018). The usage of *meioC*$^{-/-}$ ovaries enabled us to remove false positive DEG+ genes that were present as a result of oocytes contamination, and to select the transcripts expressed immediately following the onset of *foxl3* expression (Fig. 2A, B).

Fig. 2C shows the result of this screening by reverse transcription quantitative real-time polymerase chain reaction (RT-qPCR). The lower expression level of *figla* (*factor in the germline alpha*) in *meioC*$^{-/-}$ ovaries than in the wild-type ovaries indicates that the screening strategy was successful, because *figla* is expressed exclusively in oocytes (Nishimura et al., 2018). In this screening, 84 genes conserved in vertebrates were picked up from the top 200 DEG+ genes in order of significance. Four out of these 84 genes exhibited similar expression patterns to that of *foxl3*: *rec8a* (*REC8 meiotic recombination protein a*), *ces2l* (*carboxylesterase 2-like*), *atp1a3a* (*ATPase Na+/K+ transporting subunit alpha 3a*), and *fbxo47* (*F-box protein 47*). This result indicated

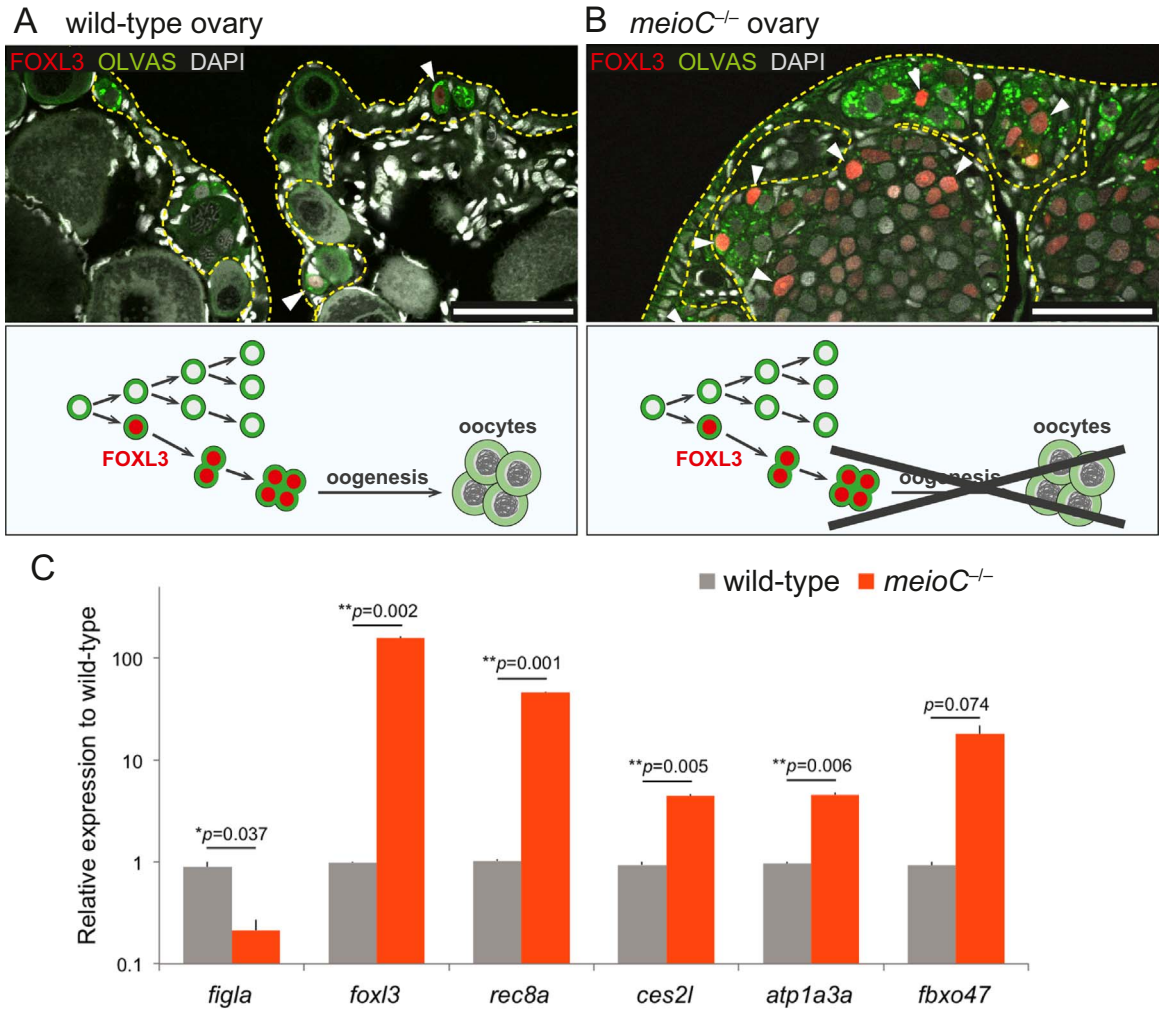

Fig. 2. RT-qPCR screening of DEGs using wild-type and *meioC*$^{-/-}$ gonads. (A, B) Germ cell development in wild-type (A) and *meioC*$^{-/-}$ (B) adult ovaries. Top panels: immunohistochemistry of ovaries. Yellow dotted lines indicate the germinal epithelium regions, where germline stem cells are present. White arrowheads indicate FOXL3-positive germ cells. Red:FOXL3; green:OLVAS; gray: DAPI. Bar:50 μm. Bottom panels: schematic representations of gametogenesis in ovaries of each genotype. (C) Relative expression levels of *figla* (oocyte marker), *foxl3*, and DEG+ candidate genes in wild-type (gray bars) and *meioC*$^{-/-}$ (orange bars) ovaries (n = 2). *Actb* was used as endogenous control. Each expression level was normalized against wild-type-1. (For interpretation of the references to color in this figure legend, the reader is referred to the web version of this article).

that these candidate genes were preferentially expressed in type I germ cells in ovaries.

2.3. Expression of the candidate DEGs in developing gonads

Because these candidate genes were isolated by detecting differences in expression levels between wild-type and *foxl3*$^{-/-}$ adult ovaries, we further confirmed the expression patterns of *rec8a*, *ces2l*, *atp1a3a*, and *fbxo47* by in situ hybridization (ISH) using female and male developing gonads.

As expected from a previous report, *foxl3* mRNA was detected in female type I and type II germ cells (Fig. 3A) but was absent in male germ cells at 15 dph (Fig. 3B) (Nishimura et al., 2015). The transcripts of *rec8a*, *atp1a3a*, and *fbxo47* were detected in type I and type II germ cells in 15 dph developing ovaries (Fig. 3C, E, G) but not in testes at the same stage (Fig. 3D, F, H). *Ces2l* was detected only in diplotene oocytes but not in mitotic type I or type II germ cells in ovaries and testes (Fig. 3I, J). Based on these results, we selected *rec8a*, *atp1a3a*, and *fbxo47* as candidates for additional investigation.

To examine the possibility that expression of *rec8a*, *atp1a3a*, and *fbxo47* are regulated downstream of *foxl3*, we performed ISH using *foxl3*$^{+/-}$ and *foxl3*$^{-/-}$ ovaries. Although all three genes were detected in mitotic germ cells of *foxl3*$^{+/-}$ ovaries (Fig. 4A, C, E), *rec8a* and *fbxo47* signals were absent in *foxl3*$^{-/-}$ ovaries (Fig. 4B, D). In contrast, *atp1a3a* expression was detected in *foxl3*$^{-/-}$ ovaries (Fig. 4F). Collectively, these results suggest that *rec8a* and *fbxo47* act downstream of *foxl3* in female mitotic germ cells.

2.4. Identification of the FOXL3-binding motif

Forkhead proteins bind to DNA by Forkhead/winged-helix domain (Harami et al., 2013). To examine whether the FOXL3 protein associates with the regulatory regions of candidate genes, we first tried to identify the FOXL3-binding motif using an improved method of DNA adenine methyltransferase identification sequencing (iDamIDseq) (Fig. 5A; Gutierrez-Triana et al., 2016). In this method, the FOXL3-binding motif was assessed by DNA adenine methyltransferase fused with FOXL3 (Dam-f-FOXL3). Injection of *Dam-f-foxl3* mRNA into fertilized eggs resulted in specific methylation at the GATC-sites around the binding motif, which was computationally extracted by comparing Dam-f-FOXL3 embryos with control embryos. As a control, Dam-fused GFP with an optimized nuclear localization signal (Dam-f-GFP) was used. Genomic DNA was purified from two day post-fertilization embryos and used for iDamIDseq.

Correlation of the read coverage over the genome was high between replicates but low between Dam-f-FOXL3 and Dam-f-GFP samples (Sup. Fig. 3), demonstrating the specificity and consistency of this method. iDEAR (iDamID Enrichment Analysis with R; Gutierrez-Triana et al.,

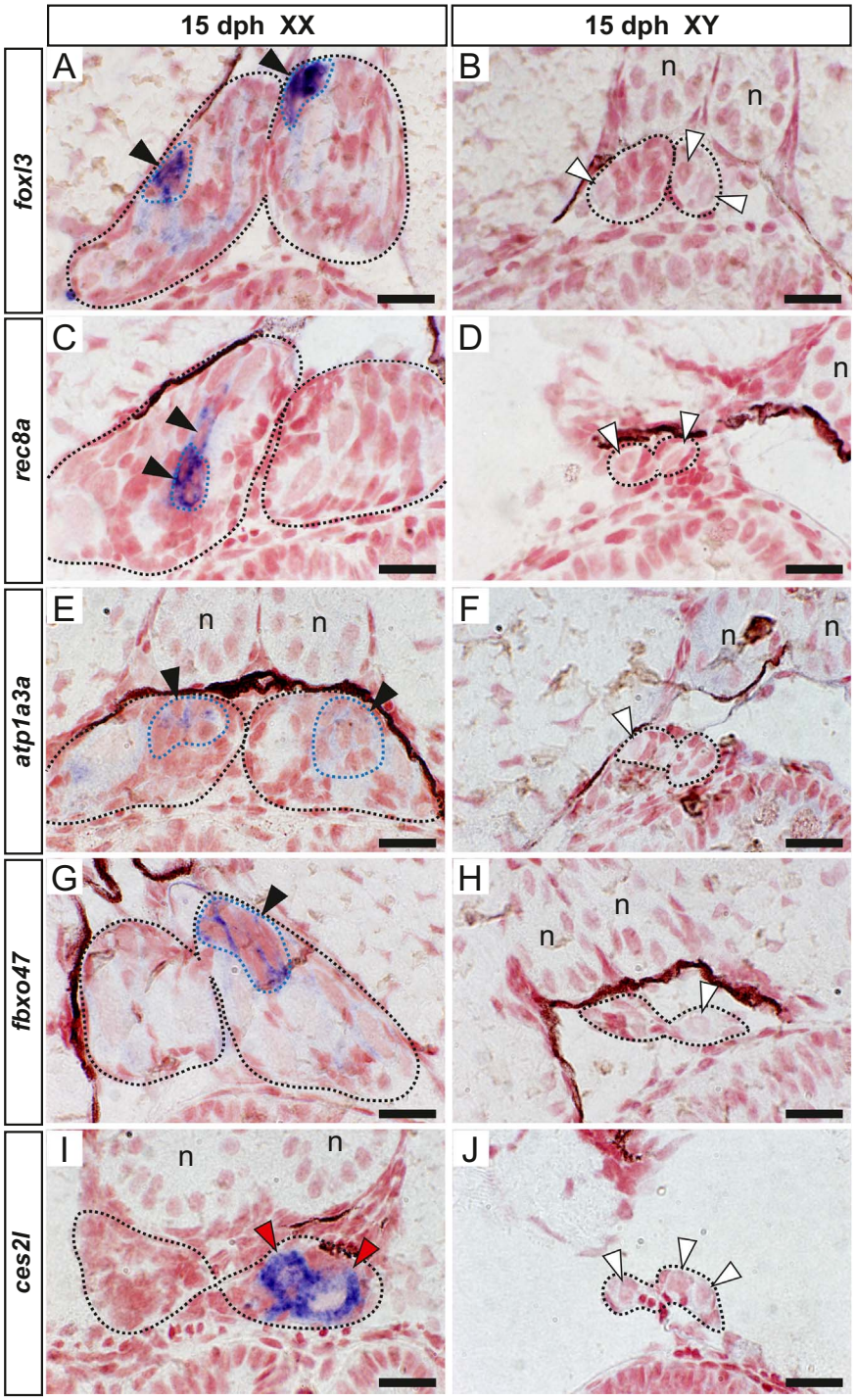

Fig. 3. Expression patterns of DEG+ genes in gonads. *In situ* hybridization of *foxl3* (A, B), *rec8a* (C, D), *atp1a3a* (E, F), *fbxo47* (G, H), and *ces2l* (I, J) using 15 dph XX (A, C, E, G, I) and XY (B, D, F, H, J) gonads. Black dashed lines indicate the outline of the gonads. Blue dashed lines within the gonads indicate type II germ cell cysts. Black and red arrowheads indicate signal-positive type I germ cells/ type II germ cell cysts and meiotic oocytes, respectively. White arrowheads indicate signal-negative germ cells. n: nephric duct. Bar: 20 μm. (For interpretation of the references to color in this figure legend, the reader is referred to the web version of this article).

2016), a package for identification of differentially methylated regions, revealed 880 significantly enriched regions in Dam-f-FOXL3 as compared to Dam-f-GFP (Fig. 5B). Using these regions as the input of DREME *de novo* motif discovery tool (Bailey, 2011), several motifs were identified in Dam-f-FOXL3-enriched regions (Fig. 5C). The most significantly enriched motif was 5′-DHAAACAA-3′ (692/880 positive regions, $p = 2.1 \times 10^{-109}$).

We confirmed FOXL3-binding affinity and specificity to the motif by electrophoretic mobility shift assay (EMSA). A mixture of nuclear extract from HeLa cells expressing His-FOXL3 protein shifted the band of a biotin-labeled FOXL3-binding motif. This shift disappeared when unlabeled FOXL3-binding motif probes were added (Fig. 5D). These results confirm that the FOXL3 protein recognizes the FOXL3-binding motif discovered by iDamIDseq.

2.5. ChIP-qPCR suggests binding of FOXL3 to candidate genes

Generally, conserved genomic regions around the transcription start site (TSS) are expected to serve as regions important for transcriptional regulation. We found conserved 5′ regions of *rec8a* and *fbxo47* among medaka, stickleback and tilapia. These regions

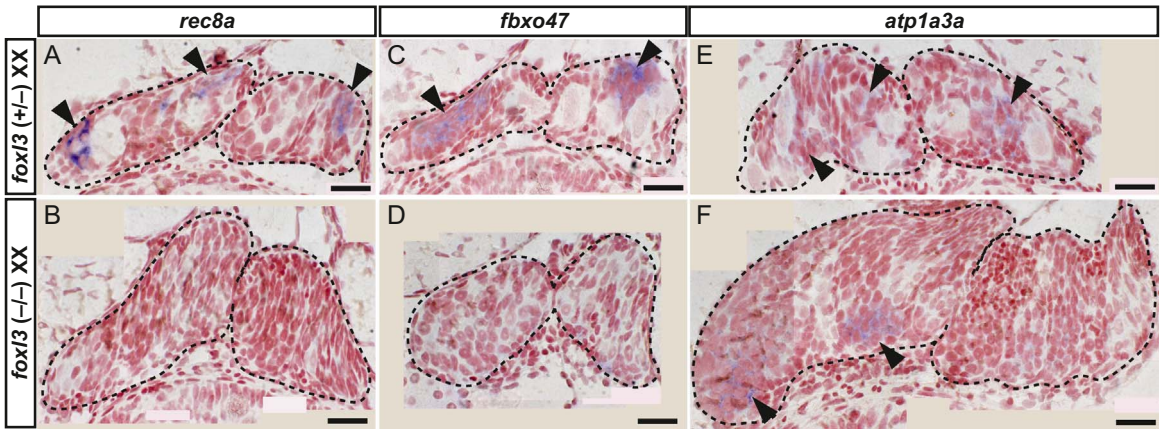

Fig. 4. Expression patterns of *rec8a*, *fbxo47*, and *atp1a3a* genes in *foxl3*-mutant gonads. *In situ* hybridization of *rec8a* (A, B), *fbxo47* (C, D), and *atp1a3a* (E, F) using 10 dph XX *foxl3*$^{+/-}$ (A, C, E) and *foxl3*$^{-/-}$ (B, D, F) gonads. Black dashed lines indicate the outline of the gonads. Black arrowheads indicate signal-positive type I germ cells/ type II germ cell cysts. Bar: 20 μm.

contained FOXL3-binding motifs (DHAAACAA, SWAAACA, AWGYAAA) (Fig. 6A, Sup. Fig. 4). The binding of FOXL3 to the conserved regions of *rec8a* and *fbxo47* was confirmed by chromatin immunoprecipitation followed by quantitative PCR (ChIP-qPCR) analyses. For this purpose, we generated anti-FOXL3 monoclonal antibodies and confirmed the affinity of the antibodies to FOXL3 by immunoprecipitation using HeLa cells transfected with a His-*foxl3* expression vector (Fig. 6B). Specificity of the antibody was verified by immunohistochemistry using developing ovaries and testes. The monoclonal antibody detected FOXL3 protein expressing in mitotic germ cells of the developing ovary but not of the developing testis as reported before (Nishimura et al., 2015) (Fig. 6C).

For FOXL3-ChIP assay, *meioC*$^{-/-}$ ovaries were used since they contain many FOXL3-positive type I germ cells (Fig. 3A, B). ChIP-qPCR results showed that FOXL3 accumulated on the putative regulatory regions of *rec8a* and *fbxo47* as compared to a negative

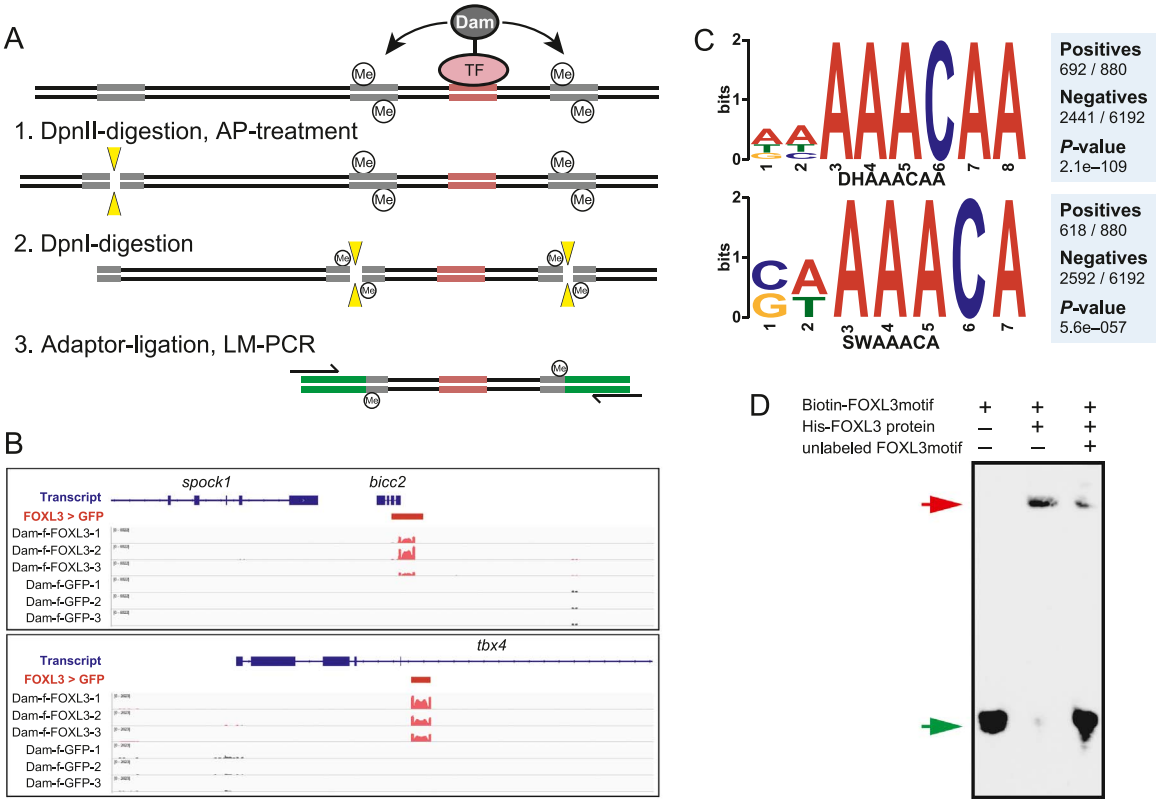

Fig. 5. Identification of FOXL3-binding motifs by iDamIDseq. (A) Schematic description of iDamIDseq. DNA adenine methyltransferase (Dam)-fused transcription factor (TF) binds to the specific binding motif on the genome (pink), following a restricted methylation of adenine of GATC sites (gray) near the binding elements. Methylated GATC sites were digested with *Dpn*I but not with *Dpn*II. Phosphorylated ends of the *Dpn*I-digested fragments were used for adaptor ligation and ligation-mediated PCR (LM-PCR) to amplify the binding motif-containing fragments for NGS library preparation. (B) Representative examples of genomic loci with significantly enriched regions derived from iDEAR (FDR < 0.05). Significance is indicated at the second line (FOXL3 > GFP). Actual read coverages of indicated samples are shown in the lower six lanes (Dam-f-FOXL3-1–3 and Dam-f-GFP-1–3). (C) FOXL3-binding motifs identified by motif-searching tool DREME. The top two motifs of a significant order are shown. (D) EMSA assay using a biotin-labeled DNA probe containing a FOXL3-binding motif sequence (Biotin-FOXL3motif), nuclear extract of HeLa: His-*foxl3* transgenic cells (His-FOXL3 protein), and unlabeled DNA probe containing a FOXL3-binding motif sequence (unlabeled FOXL3motif) used as a sequence-specific competitor of the DNA-protein interaction. Green and red arrows indicate the positions of free biotin-labeled probes and shifted biotin-labeled probes, respectively. (For interpretation of the references to color in this figure legend, the reader is referred to the web version of this article).

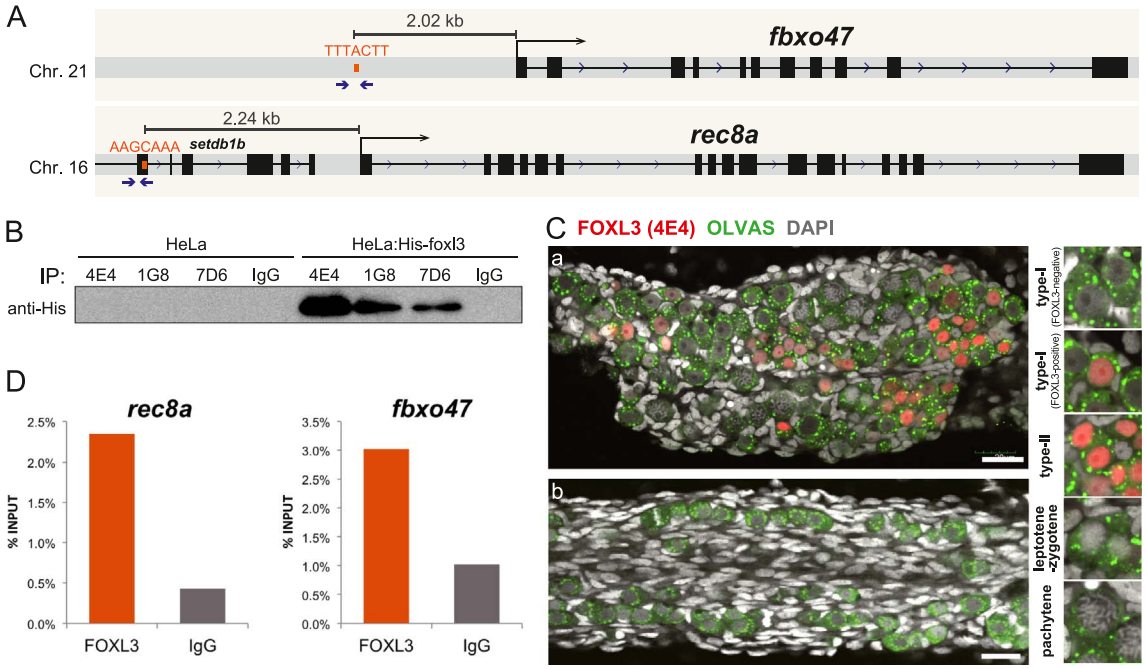

Fig. 6. ChIP-qPCR using anti-FOXL3 monoclonal antibody. (A) Schematic view of the genomic loci of *rec8a* and *fbxo47* genes. FOXL3-binding motifs within the conserved regions are shown by orange bars, and PCR primers used for ChIP-qPCR are shown by blue arrows. (B) Immunoprecipitation (IP) assay using HeLa cells transfected (HeLa: His-*foxl3*) or untransfected (HeLa) with His-*foxl3* expression vector. Anti-FOXL3 monoclonal antibodies (clone 4E4, 1G8, 7D6) or normal mouse IgG were used for IP, and an anti-His antibody was used for His-FOXL3 detection. (C) Immunohistochemistry of 10 dph wild-type ovary (a) and testis (b) using anti-FOXL3 monoclonal antibody (clone 4E4, red) anti-OLVAS antiserum (green), and DAPI (gray). Magnified images of each developmental stage of female germ cells are shown in the right five panels. Bar: 20 μm. (D) ChIP-qPCR assay using *meioC*$^{-/-}$ ovaries. Accumulation of the FOXL3 (ChIP-FOXL3) at the indicated genes' regulatory loci is indicated by "% input". As a negative control, normal mouse IgG was used for ChIP (ChIP-IgG). (For interpretation of the references to color in this figure legend, the reader is referred to the web version of this article).

control precipitated with normal mouse IgG (Fig. 6D). Combined with mRNA expression patterns, our data suggest that FOXL3 is associated with genomic regions of *rec8a* and *fbxo47* via FOXL3-binding motif and regulates their transcription in mitotic germ cells in ovaries.

3. Discussion

In this study, we have comprehensively addressed *foxl3*-downstream genes by comparing transcriptomes of mitotic germ cells between wild-type and *foxl3*$^{-/-}$. Among them, *rec8a* and *fbxo47* were expressed in mitotic germ cells in wild-type ovaries but not in *foxl3*$^{-/-}$ ovaries. We also discovered the FOXL3-binding motif by iDamIDseq-iDEAR, and found the motif within the conserved regions of *rec8a* and *fbxo47*. FOXL3 is associated with the gene loci containing the FOXL3-binding motif as indicated by ChIP-qPCR. Therefore, it is very likely that *rec8a* and *fbxo47* act downstream of *foxl3* in female mitotic germ cells during germline sex determination.

The FOXL3-binding motif identified in this study was quite similar to the Forkhead consensus motif: 5′-(G/A)(T/C)(A/C)AA(C/T)A-3′ (Fig. 4D; Georges et al., 2010), in line with the fact that the DNA-binding domain (Forkhead-domain) is highly conserved among the Forkhead family members. Interestingly, the complexity of the binding motif is not high. Therefore, other co-factors or chromatin modifications likely help to secure high target specificity (Georges et al., 2010). It is interesting to speculate that FOXL3 may function as a selective switch by acting as a pioneer factor with different partners and modulating chromatin structure. Actually another protein belonging to the Forkhead family, FoxA (also known as PHA-4), directly binds to nucleosomal DNA and initiates regulatory events, even in silent chromatin (Zaret and Mango, 2016).

Rec8a is one of two fish homologs of mammalian *Rec8*, a meiosis-specific component of cohesin complex. *Rec8* is widely conserved in eukaryotes, and is crucial not only for sister chromatid cohesion, but also for the proper association of homologous chromosomes and recombination during meiosis (Rankin, 2015). In mice, Rec8 protein is loaded onto chromatin during pre-meiotic S phase (Rankin, 2015) and chromatin cohesion in fetal oocytes is maintained for months without detectable turnover of Rec8 (Burkhardt et al., 2016). In medaka, *rec8a* mRNA was detected in female mitotic germ cells but was not detected in meiotic oocytes (Fig. 3C, D), suggesting that *rec8a* was transcribed before entering meiosis and REC8A proteins on chromatin might be stable during meiosis, consistent with the mouse results. Surprisingly, *rec8a* expression was not detected in *foxl3*$^{-/-}$ XX germ cells (Fig. 4B), indicating that *rec8a* is not required for spermatogenesis in *foxl3*$^{-/-}$ ovaries. It is possible that another *Rec8* homolog, *rec8b*, is involved in meiotic chromosome behavior during spermatogenesis.

Fbxo47 is a member of the F-box only (FBXO) gene family. F-box protein is a substrate-recognition subunit of SCF (Skp1/Cullin/F-box-protein) ubiquitin E3 ligase complex (Cardozo and Pagano, 2004). SCF complex plays a central role in various phases of the cell cycle by degrading cell cycle regulators such as Emi1 and p27 (Cardozo and Pagano, 2004). It is possible to speculate that the regulation of any mitotic process during cystic cell division in type II germ cells may have something to do with sexual fate decision. It is interesting to note several recent reports on the important roles of F-box proteins in chromosomal arrangements in germ cells. In *C. elegans*, *prom-1* (*progression of meiosis*), a homolog of *fbxo47*, is required for homologous pairing during meiotic prophase-I (Jantsch et al., 2007). In rice (*Oryza sativa*), two F-box proteins, MOF (MEIOTIC F-BOX) and ZYGO1 (ZYGOTENE 1), are essential for male-specific double-strand break repair and zygotene bouquet formation, respectively (He et al., 2016; Zhang et al., 2017). In our study, we showed female-specific and FOXL3-associated upregulation of *fbxo47* in mitotic germ cells. *Fbxo47* might regulate chromosomal behavior and/or mitotic processes to suppress initiation of spermatogenesis downstream of FOXL3.

Two *foxl3*-downstream genes identified in this study are widely

conserved in sexually reproducing organisms. Intriguingly, both of these genes could be associated with chromosomal configuration in germ cells as described above. Further studies on *rec8a* and *fbxo47* function will provide novel insight into the mechanisms of germline sex determination.

4. Material and methods

4.1. Ethics statement

All experimental procedures were performed according to the Regulations on Animal Experiments in of Nagoya University. The experimental plan using medaka was approved by the Nagoya University official ethics committee (Approval Number 20 in Department of Science, Nagoya University).

4.2. Fish

The OKcab strain of medaka fish (*Oryzias latipes*) was used in this study. Fishes were maintained in fresh water at 29 °C under photoperiodically regulated conditions (14 h light and 10 h dark).

A bacterial artificial chromosome (BAC) transgenic method was used to generate a *foxl3*-EGFP reporter construct as previously described (Nakamura et al., 2008b; Nishimura et al., 2018). A fosmid containing the *foxl3* genomic region (clone name: GOLWFno345_a19) was obtained from National BioResource Project (NBRP) Medaka (https://shigen.nig.ac.jp/medaka/). *Foxl3* 3′UTR was amplified from NBRP cDNA clone (clone name: olgi46a18; Nishimura et al., 2015), and was cloned into the hsGBA-NKm vector (Nakamura et al., 2008b) using In-Fusion HD Cloning Kit (Clontech; Mountain View, CA, USA). The resultant vector was amplified using *foxl3*-BACF and *foxl3*-BACR primers to generate the fosmid-targeting DNA fragment. After homologous recombination, the fosmid containing EGFP-*foxl3* 3′UTR-BGHpA was used for microinjection as previously described (Nakamura et al., 2008a). Primers used for the construction are listed in Supplemental Table 3.

The *foxl3*$^{-/-}$; *foxl3p*-EGFP fish was generated by crossing *foxl3*$^{-/-}$ XY males (Nishimura et al., 2015) and *foxl3p*-EGFP XX females (this paper). The *foxl3*$^{+/-}$; *foxl3p*-EGFP males and females were further intercrossed to obtain *foxl3*$^{-/-}$; *foxl3p*-EGFP and *foxl3*$^{+/+}$; *foxl3p*-EGFP XX females for RNA-sequencing library preparation.

4.3. RNA sequencing

Foxl3$^{-/-}$; *foxl3p*-EGFP or *foxl3*$^{+/+}$; *foxl3p*-EGFP XX ovaries of 3-month-old fish were used for RNA sequencing (n = 6/sample). Three replicates were prepared for each genotype. Isolated ovaries were cut into small pieces (about 1 mm square) in balanced salt solution (BSS) (Yang and Tiersch, 2009). Ovarian pieces were incubated in dissociation medium containing 0.2% collagenase type II (Worthington Biochemical Corporation; Lakewood, NJ, USA) and 0.1% trypsin (Worthington Biochemical Corporation) in Iwamatsu's saline (111.2 mM NaCl, 5.4 mM KCl, pH 7.3; Iwamatsu, 1973) at 29 °C for 2 h with pipetting every 15 min. The dissociated samples were then filtered through 37 μm-pore nylon mesh to remove undissociated tissue fragments, and the cells were resuspended in Leiboviz's L-15 medium without phenol red (Thermo Fisher Scientific; Waltham, MA, USA), supplemented with 10% fetal bovine serum (MilliporeSigma; Burlington, MA, USA), 100 U/mL penicillin–100 μg/mL streptomycin (Thermo Fisher Scientific), and 10 mM Hepes, pH 7.9 (Nacalai Tesque; Kyoto, Japan) to stop the enzymatic reaction. The suspension was filtered through 35 μm-pore cell strainer (Falcon Scientific; Seaton Delaval, UK) to disperse cells just before sorting using a cell sorter SH800 (SONY Biotechnology; San Jose, CA, USA). *Foxl3p*-EGFP-positive cells were isolated by a cell sorter according to fluorescence intensity (Sup. Fig. 1). Total RNA was extracted from 2500–4000 cells (wild-type) or 5000–10,000 cells (*foxl3*$^{-/-}$) using RNAqueous-Micro Total RNA Isolation Kit (Thermo Fisher). Between 1 and 20 ng of total RNA sample was used for Quartz-seq library preparation as described previously (Sasagawa et al., 2013). Multiplex, paired-end DNA sequencing libraries were prepared using KAPA Hyper Prep Kit for Illumina (KAPA Biosystems; Wilmington, MA, USA) and TruSeq LT adaptors (Illumina; San Diego, CA, USA). Library quality was confirmed by Agilent High Sensitivity DNA Kit (Agilent Technologies; Santa Clara, CA, USA) and KAPA library quantification kit (KAPA Biosystems). Sequencing analysis was performed using Illumina's HiSeq. 1500 sequencing machine.

4.4. Data analysis

A reference genome for Cab-strain (CabToHdrR) was created by applying variants for Cab-strain to the latest version of the reference genome for HdrR-strain (version 2.2.4) (http://utgenome.org/medaka_v2/). Comprehensive gene annotation was created by merging known annotation data (oryLat2 assembly) with other public sequences (ESTs, and cDNA sequences). Genome coordinates for annotated genes (oryLat2) were converted to those for CabToHdrR by using the UCSC LiftOver tool. Reads were mapped to CabToHdrR genome using the Subjunc read aligner (v1.5.1) (Liao et al., 2013) and supplying gene annotation data. The number of total mapped reads were approximately 7–13 million. Mapped reads were counted and analyzed for differentially expressed genes using edgeR (Robinson et al., 2010).

Functional annotation clustering of enriched gene ontology terms was analyzed by The Database for Annotation, Visualization, and Integrated Discovery (DAVID) (Huang et al., 2009; https://david.ncifcrf.gov).

4.5. RT-qPCR

Total RNA was isolated from one wild-type ovary or three *meioC*$^{-/-}$ ovaries using TriPure Isolation Reagent (MilliporeSigma), according to the manufacturer's protocol. For each genotype, two independent experiments were performed. SuperScript III Reverse Transcriptase (Thermo Fisher Scientific) was used for cDNA synthesis. qPCR was performed using KOD SYBR qPCR Mix (TOYOBO; Osaka, Japan) and StepOnePlus real-time PCR system (Thermo Fisher). Cycling parameters were: 95 °C for 10 min; 40 cycles of 95 °C for 15 s and 60 °C for 1 min. Primers used for qPCR are shown in Table 3.

4.6. In situ hybridization and immunohistochemistry

Whole-mount in situ hybridization and immunohistochemistry were performed as previously described (Oliver et al., 1996; Nakamura et al., 2006; Nishimura et al., 2018). cDNA clones for *foxl3* (olgi46a18), *atp1a3a* (olbr29a24), *fbxo47* (olte61d07), and *ces2l* (olvl64m02) were obtained from NBRP Medaka. *Rec8a* cDNA was cloned from total cDNA of *meioC*-mutant ovaries (Nishimura et al., 2018). The cDNAs were used as templates to amplify T7-tagged PCR fragments (primers shown in Supplemental Table 3). Images were obtained using the Olympus BX50WI upright microscope and Olympus DP70 CCD camera (Olympus Corporation; Tokyo, Japan).

For immunohistochemistry, anti-OLVAS (medaka VASA antibody, 1:200, rat; Aoki et al., 2008), anti-GFP (1:100, mouse; Clontech) and anti-FOXL3 (1:200, mouse; medaka FOXL3 antibody generated in this study as described below) were used as primary antibodies. The primary antibodies were detected by Alexa Fluor 488, Alexa Fluor 568, and Alexa Fluor 647-conjugated secondary antibodies (1:100, goat; Thermo Fisher Scientific). Images were obtained using the Olympus FLUOVIEW FV1000 confocal microscope.

4.7. iDamIDseq-iDEAR

Methods for iDamIDseq-iDEAR, including library preparation, deep sequencing, and data processing were described previously (Gutierrez-Triana et al., 2016).

pCS2 + DamL122A-f-mmGFPoN plasmid vector contains the coding sequence of DamL122A (a mutant version of Dam, referred to as Dam) fused with a flexible linker (f) and monomeric GFP with an optimized nuclear localizing signal (mmGFPoN) (referred to as *Dam-f-GFP*). We replaced the mmGFPoN with *foxl3* ORF (*Dam-f-foxl3*) using *Spe*I and *Xba*I restriction enzymes. Primers used for the construction are listed in Supplemental Table 3.

Dam-f-GFP and *Dam-f-foxl3* mRNAs were synthesized using mMESSAGE mMACHINE SP6 Transcription kit (Thermo Fisher Scientific), and injected into 1-cell stage medaka embryos at a concentration of 10 ng/μL. The embryos were maintained in ERM medium supplemented with 200 U/mL penicillin, 200 μg/mL streptomycin, and 0.0001% methylene blue.

Genomic DNA extraction and preparation of iDamIDseq libraries were performed as described previously (Gutierrez-Triana et al., 2016). Three replicates were prepared for each sample. For ligation-mediated PCR, the amplification step was repeated 29 times. Sequencing libraries were analyzed using an Illumina Hiseq. 2500 machine.

Sequenced reads were mapped on the medaka genome (CabToHdrR). Fifty to seventy million reads were uniquely mapped on the genome, and used in iDEAR 2.0. Dam-f-FOXL3-enriched regions were used as the input for *de novo* motif discovery using DREME (Discriminative Regular Expression Motif Elicitation; Bailey, 2011; http://meme-suite.org/doc/dreme.html).

4.8. Cell culture and establishment of HeLa: His-foxl3 cell line

HeLa cells were maintained in DMEM medium containing 10% FBS (fetal bovine serum), 100 U/mL penicillin, and 100 ng/mL streptomycin. Cells were cultivated at 37 °C in a humidified, 5% CO_2-containing atmosphere.

To establish a HeLa cell line expressing His-*foxl3* (referred as to HeLa: His-*foxl3*), a pPyCAG-*foxl3*-IP vector was constructed by inserting a His-*foxl3*-containing fragment into a pPyCAG-ME-IP vector using NotI and XhoI restriction enzymes. Primers used for the vector construction are listed in Supplemental Table 3. HeLa cells were transfected with the vector using GeneJuice Transfection Reagent (Merck; Darmstadt, Germany). Puromysin-resistant colonies were picked to establish stable cell lines.

4.9. Electrophoretic mobility shift assay (EMSA)

For EMSA, nuclear proteins were extracted from about 1×10^7 HeLa: His-*foxl3* cells using NE-PER Nuclear and Cytoplasmic Extraction Reagents (Thermo Fisher Scientific). The nuclear extract was concentrated by ultrafiltration using Vivaspin500 (GE Healthcare; Chicago, IL, USA) and dialyzed using Slide-A-Lyzer MINI Dialysis Unit (Thermo Fisher Scientific) to suspend the proteins in 60 μL dialysate containing 200 mM KCl, 10 mM Tris-HCl (pH 8.0), 2.5% glycerol, 1 mM DTT, and 0.5 mM EDTA (pH 8.0).

EMSA was performed using the LightShift Chemiluminescent EMSA Kit (Thermo Fisher Scientific) according to the manufacturer's instructions. The binding reaction mix (20 μL) contained 1X binding buffer (kit content), 2.5% glycerol, 5 mM $MgCl_2$, 1 μg Poly (dI-dC), 4 pmol unlabeled DNA probe, 2 μL nuclear extract, and 20 fmol biotin-labeled DNA probe. The reaction mix was first incubated for 10 min at room temperature without biotin-labeled DNA probes. After adding biotin-labeled DNA probes, the mixture was further incubated for 20 min at room temperature. The reaction mixture was loaded on to a 6% polyacrylamide-gel. After electrophoresis, DNA was transferred to a positively charged nylon membrane (GE Healthcare) and crosslinked to the membrane at 120 mJ/cm^2 using a UV-light crosslinker (UVP, CL-1000). The signal was detected using streptavidin-horseradish peroxidase conjugate and a chemiluminescent substrate according to the manufacturer's instructions. Chemiluminescent signals were detected by ImageQuant LAS 4000 (GE Healthcare).

4.10. Generation of anti-FOXL3 monoclonal antibody

The C-terminus region of the FOXL3 protein (a.a. 137–263, refer to as FOXL3Δ2) was used as an immunogen to generate an anti-FOXL3 monoclonal antibody. The *Foxl3*Δ2-coding sequence was cloned into a modified pET11d vector using NdeI and XhoI restriction enzymes. Primers used for the construction are listed in Supplemental Table 3.

The resultant vector was transformed to BL21(DE3)pLysS competent cells cultured in 1.6 L medium. When the bacterial OD_{600} reached 0.6, the 6xHis-FOXL3Δ2 protein was induced by culturing with 0.5 mM IPTG for 3 h. Since most of the induced protein was isolated in inclusion bodies, it was solubilized with 6 M guanidine hydrochloride and purified with 4 mL Ni-NTA agarose (QIAGEN). Next, the protein was precipitated by buffer exchange to dialysate [20 mM Tris-HCl (pH 8.0), 150 mM KCl, 10% glycerol, 0.001% NP-40] using the Spectra/Por3 dialysis membrane (FED) and the precipitant was dissolved in SDS-PAGE sample buffer. The protein was electrophoresed in a polyacrylamide gel, and the correct sized band was excised for gel-reconstitution and electroelution to obtain the highly concentrated and purified protein sample.

The mouse iliac lymph node method was employed to generate monoclonal antibodies (Sado et al., 2006). Hybridomas were screened in several ways: ELISA, immunocytochemistry using HeLa: His-foxl3 cells, and immunohistochemistry using medaka ovaries. Finally, two clones (4E4 and 1G8) that showed high affinity and specificity to FOXL3 were selected for final purification by cation exchange chromatography.

4.11. Immunoprecipitation

1×10^7 cells of HeLa and HeLa: His-*foxl3* were lysed with 1 mL RIPA (radio-immunoprecipitation assay) buffer [50 mM Tris-HCl (pH 8.0), 150 mM NaCl, 0.5% SDS, 0.1% NP-40, 1% sodium deoxycholate, and 1 mM PMSF] for 30 min on ice. Cell lysates were centrifuged at 16,000*g* for 20 min at 4 °C, and the supernatants (protein lysates) were used for immunoprecipitation.

10 μL Protein G Sepharose 4 Fast Flow (GE Health) was mixed with 300 μL TBS containing 1 μg IgG (anti-FOXL3 antibody or normal mouse IgG) overnight at 4 °C. To reduce non-specific binding of proteins to Protein G sepharose, 500 μL protein lysates were incubated with Protein G sepharose for 30 min at 4 °C, and unbound lysates were used for immunoreaction. Protein G - IgG complexes were washed with ice-cold TBS three times. Five μL Protein G - IgG sepharose was mixed with 500 μL unbound protein lysate for 60 min at 4 °C. Protein G - IgG - protein complex was washed with ice-cold TBS three times, and used for SDS-PAGE and Western blotting. Anti-His rabbit antibody (1:1000) was used as a primary antibody, and anti-rabbit-HRP conjugate (1:1000) was used to detect the primary antibody. Chemiluminescent signals were detected with Chemi-Lumi One (Nacalai Tesque) and LAS3000mini.

4.12. ChIP-qPCR

ChIP was performed using the anti-medaka FOXL3 monoclonal antibody (clone 4E4, mouse). We followed the ChIP protocols described previously (Nakamura et al., 2014) with a few modifications. Cells were isolated from three *meioC*$^{-/-}$ ovaries using a 21 G needle, and fixed with 1% formaldehyde for 10 min at room temperature (RT). The reaction was quenched by 200 mM glycine. Cells were washed with PBS containing cOmplete Protease Inhibitor (Roche; Basel,

Switzerland) and 1 mM PMSF, resuspended with Lysis buffer [50 mM Tris-HCl (pH 8.0), 10 mM EDTA, 1% SDS, cOmplete Protease Inhibitors, 1 mM PMSF]. Chromatin was sheared using the Covaris S2 ultrasonicator [duty cycle: 2%, intensity: 3, cycle/burst: 200, processing time: 60 s, cycle number: 2] (Covaris; Woburn, MA, USA), and centrifuged for collecting chromatin lysates. The chromatin lysates were diluted with RIPA buffer [10 mM Tris-HCl (pH 8.0), 140 mM NaCl, 1 mM EDTA, 0.5 mM EGTA, 1% Triton X-100, 0.1% SDS, 0.1% sodium deoxycholate, cOmplete Protease Inhibitors, 1 mM PMSF], and 10 μg of chromatin DNA was used for immunoreaction. The chromatin lysate was mixed with antibody/protein G Dynabeads complex (Thermo Fisher Scientific), and rotated overnight at 4 °C. Immunoprecipitated samples were washed with RIPA buffer and TE buffer, and lysed with lysis buffer overnight at 65 °C. The eluates were treated with RNase A for 2 h at 37 °C, and proteinase K for 2 h at 55 °C. DNA was purified with AMPure XP (Beckman Coulter; Brea, CA, USA), and quantified using Qubit dsDNA HS Assay Kit (Thermo Fisher Scientific). Input DNA was simultaneously treated from the elution step.

Input and immunoprecipitated DNAs were analyzed by qPCR using KOD SYBR qPCR Mix (TOYOBO) and StepOnePlus (Thermo Fisher Scientific) real-time PCR system. All PCR primers are listed in Supplemental Table 3.

4.13. Data availability

All sequence data have been deposited in the International Nucleotide Sequence Database Collaboration Sequence Read Archive via DNA Data Bank of Japan under ID codes DRA006391 (Quartz-seq) and DRA007212 (iDamIDseq).

Acknowledgements

We would like to thank Dr. R. Nakamura in University of Tokyo and Dr. T. Baba in Kyushu University for giving us protocols and technical advices for ChIP analysis, and Dr. Y. Miyanari in NIBB for providing pPyCAG-ME-IP vector. We thank Dr. K. Yamaguchi (NIBB) for next-generation sequencing. We are grateful to Tanaka Lab members in Nagoya University and the previous lab members in NIBB for informative suggestions, and Ms. I. Watakabe and Mr. K. Suzuki for fish maintenance. We thank NBRP Medaka for providing cDNAs. This work was supported by a Research Fellowships of Japan Society for the Promotion of Science for Young Scientists (16J16351:MK), a Grant-in-Aid for Young Scientists (B) (16K18557:TN), a Grant-in-Aid for Scientific Research on Innovative Areas (17H06430: MT) and a Grant-in-Aid for Scientific Research (A) (16H02514: MT). This work was supported by NIBB Collaborative Research (17-420).

Competing interests

The authors declare no competing financial interests.

Appendix A. Supporting information

Supplementary data associated with this article can be found in the online version at doi:10.1016/j.ydbio.2018.10.019.

References

Adolfi, M.C., Herpin, A., Regensburger, M., Sacquegno, J., Waxman, J.S., Schartl, M., 2016. Retinoic acid and meiosis induction in adult versus embryonic gonads of medaka. Sci. Rep. 6, 34281. http://dx.doi.org/10.1038/srep34281.

Aoki, Y., Nagao, I., Saito, D., Ebe, Y., Kinjo, M., Tanaka, M., 2008. Temporal and spatial localization of three germline-specific proteins in medaka. Dev. Dyn. 237 (3), 800–807. http://dx.doi.org/10.1002/dvdy.21448.

Aoki, Y., Nakamura, S., Ishikawa, Y., Tanaka, M., 2009. Expression and syntenic analysis of four nanos genes in medaka. Zool. Sci. 26 (2), 112–118. http://dx.doi.org/10.2108/zsj.26.112.

Bailey, T.L., 2011. DREME: motif discovery in transcription factor ChIP-seq data. Bioinfomatics 27 (12), 1653–1659. http://dx.doi.org/10.1093/bioinformatics/btr261.

Beer, R.L., Draper, B.W., 2013. nanos3 maintains germline stem cells and expression of the conserved germline stem cell gene nanos2 in the zebrafish ovary. Dev. Biol. 374 (2), 308–318. http://dx.doi.org/10.1016/j.ydbio.2012.12.003.

Bertho, S., Pasquier, J., Pan, Q., Trionnaire, G.L., Bobe, J., Postlethwait, J.H., Pailhoux, E., Schartle, M., Herpin, A., Guiguen, Y., 2016. Foxl2 and its relatives are evolutionary conserved players in gonadal sex differentiation. Sex. Dev. 10 (3), 111–129. http://dx.doi.org/10.1159/000447611.

Bowles, J., Koopman, P., 2007. Retinoic acid, meiosis and germ cell fate in mammals. Development 134 (19), 3401–3411. http://dx.doi.org/10.1242/dev.001107.

Bowles, J., Koopman, P., 2010. Sex determination in mammalian germ cells: extrinsic versus intrinsic factors. Reproduction 139 (6), 943–958. http://dx.doi.org/10.1530/REP-10-0075.

Burkhardt, S., Borsos, M., Szydlowska, A., Godwin, J., Williams, S.A., Cohen, P.E., Hirota, T., Saitou, M., Tachibana-Konwalski, K., 2016. Chromosome cohesion established by Rec8-cohesion in fetal oocytes is maintained without detectable turnover in oocytes arrested for months in mice. Curr. Biol. 26 (5), 678–685. http://dx.doi.org/10.1016/j.cub.2015.12.073.

Cardozo, T., Pagano, M., 2004. The SCF ubiquitin ligase: insights into a molecular machine. Nat. Rev. Mol. Cell Biol. 5 (9), 739–751. http://dx.doi.org/10.1038/nrm1471.

Georges, A.B., Benayoun, B.A., Caburet, S., Veitia, R.A., 2010. Generic binding sites, generic DNA-binding domains: where does specific promoter recognition come from? FASEB J. 24 (2), 346–356. http://dx.doi.org/10.1096/fj.09-142117.

Gutierrez-Triana, J.A., Mateo, J.L., Ibberson, D., Ryu, S., Wittbrodt, J., 2016. iDamIDseq and iDEAR: an improved method and computational pipeline to profile chromatin-binding proteins. Development 143 (22), 4272–4278. http://dx.doi.org/10.1242/dev.139261.

Harami, G.M., Gyimesi, M., Kovacs, M., 2013. From keys to bulldozers: expanding roles for winged helix domains in nucleic-acid-binding proteins. Trends Biochem. Sci. 38 (7), 364–371. http://dx.doi.org/10.1016/j.tibs.2013.04.006.

He, Y., Wang, C., Higgins, J.D., Yu, J., Zong, J., Lu, P., Zhang, D., Liang, W., 2016. MEIOTIC F-BOX is essential for male meiotic DNA double-strand break repair in rice. Plant Cell 28 (8), 1879–1893. http://dx.doi.org/10.1105/tpc.16.00108.

Huang, D.W., Sherman, B.T., Lempicki, R.A., 2009. Systematic and integrative analysis of large gene lists using DAVID bioinformatics resources. Nat. Protoc. 4 (1), 44–57. http://dx.doi.org/10.1038/nprot.2008.211.

Iwamatsu, T., 1973. Studies on oocyte maturation in the medaka, Oryzias latipes. -Improvement of culture medium for oocytes in vitro. Jpn. J. Ichthyol. 20 (4), 218–224.

Jantsch, V., Tang, L., Pasierbek, P., Penkner, A., Nayak, S., Baudrimont, A., Schedl, T., Gartner, A., Loidl, J., 2007. Caenorhabditis elegans prom-1 is required for meiotic prophase progression and homologous chromosome pairing. Mol. Biol. Cell 18 (12), 4911–4920. http://dx.doi.org/10.1091/mbc.E07-03-0243.

Kato, Y., Katsuki, T., Kokubo, H., Masuda, A., Saga, Y., 2015. Dazl is a target RNA suppressed by mammalian NANOS2 in sexually differentiating male germ cells. Nat. Commun. 7, 11272. http://dx.doi.org/10.1038/ncomms11272.

Liao, Y., Smyth, G.K., Shi, W., 2013. The subread aligner: fast, accurate and scalable read mapping by seed-and-vote. Nucleic Acids Res. 41 (10), e108. http://dx.doi.org/10.1093/nar/gkt214.

Miyauchi, H., Ohta, H., Nagaoka, S., Nakaki, F., Sasaki, K., Hayashi, K., Yabuta, Y., Nakamura, T., Yamamoto, T., Saitou, M., 2017. Bone morphogenetic protein and retinoic acid synergistically specify female germ-cell fate in mice. EMBO J. 36 (21), 3100–3119. http://dx.doi.org/10.15252/embj.201796875.

Nakamura, R., Tsukahara, T., Qu, W., Ichikawa, K., Otsuka, T., Ogoshi, K., Saito, T.L., Matsushima, K., Sugano, S., Hashimoto, S., Suzuki, Y., Morishita, S., Takeda, H., 2014. Large hypomethylated domains serve as strong repressive machinery for key developmental genes in vertebrates. Development 141 (13), 2568–2580. http://dx.doi.org/10.1242/dev.108548.

Nakamura, S., Kobayashi, D., Aoki, Y., Yokoi, H., Ebe, Y., Wittbrodt, J., Tanaka, M., 2006. Identification and liniage tracing of two populations of somatic gonadal precursors in medaka embryos. Dev. Biol. 295 (2), 678–688. http://dx.doi.org/10.1016/j.ydbio.2006.03.052.

Nakamura, S., Aoki, Y., Saito, D., Kuroki, Y., Fujiyama, A., Naruse, K., Tanaka, M., 2008a. Sox9b/sox9a2-EGFP transgenic medaka reveals the morphological reorganization of the gonads and a common precursor of both the female and male supporting cells. Mol. Reprod. Dev. 75 (3), 472–476. http://dx.doi.org/10.1002/mrd.20764.

Nakamura, S., Saito, D., Tanala, M., 2008b. Generation of transgenic medaka using modified bacterial artificial chromosome. Dev. Growth Differ. 50 (6), 415–419. http://dx.doi.org/10.1111/j.1440-169X.2008.01027.x.

Nakamura, S., Kobayashi, K., Nishimura, T., Higashijima, S., Tanaka, M., 2010. Identification of germline stem cells in the ovary of the teleost medaka. Science 328 (5985), 1561–1563. http://dx.doi.org/10.1126/science.1185473.

Nishimura, T., Sato, T., Yamamoto, Y., Watakabe, I., Ohkawa, Y., Suyama, M., Kobayashi, S., Tanaka, M., 2015. Foxl3 is a germ cell-intrinsic factor involved in sperm-egg fate decision in medaka. Science 349 (6245), 328–331. http://dx.doi.org/10.1126/science.aaa2657.

Nishimura, T., Yamada, K., Fujimori, C., Kikuchi, M., Kawasaki, T., Siegfried, K., Sakai, N., Tanaka, M., 2018. Germ cells in the teleost fish medaka have an inherent feminizing effect. PLoS Genet. 14 (3), e1007259. http://dx.doi.org/10.1371/journal.pgen.1007259.

Oliver, G., Loosli, F., Köster, R., Wittbrodt, J., Gruss, P., 1996. Ectopic lens induction in fish in response to the murine homeobox gene Six3. Mech. Dev. 60 (2), 233–239.

Rankin, S., 2015. Complex elaboration: making sense of meiotic cohesin dynamics. FEBS J. 282 (13), 2426–2443. http://dx.doi.org/10.1111/febs.13301.

Robinson, M.D., McCarthy, D.J., Smyth, G.K., 2010. edgeR: a bioconductor package for differential expression data. Bioinformatics 26 (1), 139–140. http://dx.doi.org/10.1093/bioinformatics/btp616.

Sado, Y., Inoue, S., Tomono, Y., Omori, H., 2006. Lymphocytes from enlarged iliac lymph nodes as fusion partners for the production of monoclonal antibodies after a single tail base immunization attempt. Acta Histochem. Cytochem. 39 (3), 89–94. http://dx.doi.org/10.1267/ahc.06001.

Saito, D., Morinaga, C., Aoki, Y., Nakamura, S., Mitani, H., Furutani-Seki, M., Kondoh, H., Tanaka, M., 2007. Proliferation of germ cells during gonadala sex differentiation in medaka: insights from germ cell-depleted mutant zenzai. Dev. Biol. 310 (2), 280–290. http://dx.doi.org/10.1016/j.ydbio.2007.07.039.

Sasagawa, Y., Nikaido, I., Hayashi, T., Danno, H., Uno, K.D., Imai, T., Ueda, H.R., 2013. Quartz-seq: a highly reproducible and sensitive single-cell RNA sequencing method, reveals non-genetic gene-expression heterogeneity. Genome Biol. 14 (4), R31. http://dx.doi.org/10.1186/gb-2013-14-4-r31.

Tanaka, M., 2016. Germline stem cells are critical for sexual fate decision of germ cells. Bioessays 38 (12), 1227–1233. http://dx.doi.org/10.1002/bies.201600045.

Wu, Q., Fukuda, K., Kato, Y., Zhou, Z., Deng, C.X., Saga, Y., 2016. Sexual fate change of XX germ cells caused by the deletion of SMAD4 and STRA8 independent of somatic sex reproduction. PLoS Biol. 14 (9), e1002553. http://dx.doi.org/10.1371/journal.pbio.1002553.

Yang, H., Tiersch, T.R., 2009. Current status of sperm cryopreservation in biomedical research fish models: zebrafish, medaka, and Xiphophorus. Comp. Biochem. Physiol. C Toxicol. Pharmacol. 149 (2), 224–2322. http://dx.doi.org/10.1016/j.cbpc.2008.07.005.

Zaret, K.S., Mango, S.E., 2016. Pioneer transcription factors, chromatin dynamics, and cell fate control. Curr. Opin. Genet. Dev. 37, 76–81. http://dx.doi.org/10.1016/j.gde.2015.12.003.

Zhang, F., Tang, D., Shen, Y., Xue, Z., Shi, W., Ren, L., Du, G., Li, Y., Cheng, Z., 2017. The F-box protein ZYGO1 mediates bouquet formation to promote homologous pairing, synapsis, and recombination in rice meiosis. Plant Cell 29 (10), 2597–2609. http://dx.doi.org/10.1105/tpc.17.00287.